

DISCOVERY OF NEVII IN THE WINDS OF HOT EVOLVED STARS*

J.E. HERALD, L. BIANCHI

Center for Astrophysical Sciences, The Johns Hopkins University

D.J. HILLIER

Department of Physics and Astronomy, The University of Pittsburgh

Draft version November 17, 2018

ABSTRACT

We show that a strong P-Cygni feature seen in the far-UV spectra of some very hot ($T_{eff} \gtrsim 85$ kK) central stars of planetary nebulae (CSPN), which has been previously identified as C III $\lambda 977$, actually originates from Ne VII $\lambda 973$. Using stellar atmospheres models, we reproduce this feature seen in the spectra of two [WR]-PG 1159 type CSPN, Abell 78 and NGC 2371, and in one PG 1159 CSPN, K 1-16. In the latter case, our analysis suggests an enhanced neon abundance. Strong neon features in CSPN spectra are important because an overabundance of this element is indicative of processed material that has been dredged up to the surface from the inter-shell region in the “born-again” scenario, an explanation of hydrogen-deficient CSPN. Our modeling indicates the Ne VII $\lambda 973$ wind feature may be used to discern enhanced neon abundances for stars showing an unsaturated P-Cygni profile, such as some PG 1159 stars. We explore the potential of this strong feature as a wind diagnostic in stellar atmospheres analyses for evolved objects. For the [WR]-PG 1159 objects, the line is present as a P-Cygni line for $T_{eff} \gtrsim 85$ kK, and becomes strong for $100 \lesssim T_{eff} \lesssim 155$ kK when the neon abundance is solar, and can be significantly strong beyond this range for higher neon abundances. When unsaturated, *i.e.*, for very high T_{eff} and/or very low mass-loss rates, it is sensitive to \dot{M} and very sensitive to the neon abundance. The Ne VII classification is consistent with recent identification of this line seen in absorption in many PG 1159 spectra.

Subject headings: stars: atmospheres — stars: Wolf-Rayet — stars: individual (NGC 2371, Abell 78, K 1-16)
— planetary nebulae: general — UV: spectroscopy

1. INTRODUCTION

Central stars of planetary nebulae (CSPN) represent an evolutionary phase the majority of low/intermediate mass stars will experience. A small subset of CSPN have been termed “PG 1159-[WR]” stars, as they represent objects transitioning from the [WR] to the PG 1159 class. The former are objects moving along the constant-luminosity branch of the H-R diagram which have optical spectra rich in strong emission line features, similar to those of Wolf-Rayet (WR) stars, which represent a late evolutionary stage of massive stars (the “[WR]” designation is meant to distinguish the two). The majority of [WR] CSPN show prominent carbon features and are termed “[WC]”, while a handful show strong oxygen lines (“[WO]”). This difference is believed to reflect a difference in the ionization of the winds rather than in the elemental abundances (Crowther et al. 2002). Unlike massive WR stars, CSPN of the nitrogen-rich [WN] subtype are very rare, the two candidates being LMC-N66 in the LMC (Peña et al. 2004) and PM5 in the Galaxy (Morgan et al. 2003). The PG 1159 class marks the entry point onto the white-dwarf cooling sequence, and these stars display mainly absorption line profiles in the optical, as their stellar wind has almost all but faded. Both classes are examples of hydrogen-deficient CSPN, which presumably make up 10-20% of the CSPN population (De Marco & Soker 2002; Koesterke & Werner 1998 and references therein), and are believed to represent sub-

sequent evolutionary stages based on their similar parameters and abundances. An explanation for the origin of such objects is the “born-again” scenario (see Iben & McDonald 1995; Herwig et al. 1999 and references therein). In this scenario, helium shell flashes produce processed material between the H- and He-burning shells (the intershell region). This material is enriched in He from CNO hydrogen burning, but through 3α process burning it also becomes enriched in C, O, Ne, and deficient in Fe (see, *e.g.*, Werner et al. 2004, and references therein). After the star initially moves off the asymptotic giant-branch (AGB), it experiences a late helium-shell flash, causing the star to enter a second (or “born-again”) AGB phase. Flash induced mixing dredges the processed intershell material to the surface, resulting in H-deficient surface abundances. When the star enters its second post-AGB phase, its spectrum can develop strong wind features causing it to resemble that of (massive) WR stars, perhaps because the chemically enriched surface material increases the efficiency of radiative momentum transfer to the wind. Eventually, as the wind fades, the object moves onto the white dwarf cooling sequence. As this happens, observable wind spectral features may only be present in the far-UV and UV regions.

Herald & Bianchi (2004b) (hereafter, HB04) modeled the far-UV and UV spectra of four Galactic CSPN, including Abell 78 (A78 hereafter), considered the proto-typical transition star and candidate for the born-again scenario. Crowther et al. (1998) classified it as a PG 1159-[WO1] star based on its high O VI/C IV ratio. HB04 also presented an analysis of NGC 2371, which the authors argue is of similar nature, although possessing a wind of even higher ionization. In those analyses, HB04 were unable to reproduce the promi-

*BASED ON OBSERVATIONS MADE WITH THE NASA-CNES-CSA FAR ULTRAVIOLET SPECTROSCOPIC EXPLORER AND DATA FROM THE MAST ARCHIVE. FUSE IS OPERATED FOR NASA BY THE JOHNS HOPKINS UNIVERSITY UNDER NASA CONTRACT NAS5-32985.

ment P-Cygni feature seen in the spectra of both stars at $\sim 975 \text{ \AA}$, identified in the spectra of A78 as C III $\lambda 977$ in the past (Koesterke & Werner 1998). Prominent C III $\lambda 977$ P-Cygni profiles do occur in the far-UV spectra of CSPN of cooler temperatures ($T_{eff} \lesssim 80 \text{ kK}$, see, *e.g.*, Herald & Bianchi 2004a), as well as in massive hot stars. However, effective temperatures of the transition objects (such as A78) are found to be very high (*i.e.*, $\gtrsim 90 \text{ kK}$) from both stellar atmospheres codes (*e.g.*, Werner et al. 2003, HB04) and nebular line analyses (*e.g.*, Kaler et al. 1993; Grewing & Neri 1990). HB04 noted that although this feature has been assumed to be from C III, a strong transition from an ion of relatively low ionization potential (48 eV) in such highly-ionized winds was strongly questionable. HB04 investigated and excluded the possibility that the line originated from a highly ionized iron species.

Werner et al. (2004) reported the identification of a narrow absorption feature at $\lambda 973$ in the spectra of several PG 1159 stars as Ne VII. In some cases, this line is superimposed on a broad P-Cygni feature, which they identified as C III $\lambda 977$. Given that the high ionization potential of Ne VII (207 eV) is more consistent with the conditions expected in objects of such high temperatures, we were motivated to include neon in the model atmospheres of A78 and NGC 2371 presented in HB04. Neon had not been included in any previous modeling. We present the results of this analysis, and report that neon can adequately account for this hitherto unexplained wind feature. Additionally, we show that Ne VII is also responsible for the broad P-Cygni feature seen in the spectra of the PG 1159 star K 1-16. We also investigate, with a grid of models, the usefulness of this line as a wind diagnostic for very hot CSPN. As the neon abundance is also of interest with respect to massive stars with winds, this work may have application to the study of the hottest Wolf-Rayet stars as well. This paper is arranged as follows: the observations are described in § 2. The models are described in § 3. Our results are discussed in § 4 and our conclusions in § 5.

2. OBSERVATIONS AND REDUCTION

The data sets utilized in this paper are summarized in Table 1. For NGC 2371 and K 1-16, we have used far-UV data from *Far-Ultraviolet Spectroscopic Explorer* (FUSE), and for A78, from the *Berkeley Extreme and Far-UV Spectrometer* (BEFS). For NGC 2371, we have also made use of a UV *International Ultraviolet Explorer* (IUE) spectrum. The data characteristics, and the reduction of the FUSE data, are described in HB04. The data were acquired from the MAST archive.

For K 1-16, the FUSE data were reduced in a similar manner as described in HB04, except with the latest version of the FUSE pipeline (CALFUSE v2.4). The count-rate plots show that the star was apparently out of the aperture during part of the observation, and data taken during that period was omitted from the reduction process.

The radial velocities of NGC 2371 and A78 are $+20.6$ and $+17 \text{ km s}^{-1}$, respectively (Acker et al. 1992). All observed spectra presented in this paper have been velocity-shifted to the rest-frame of the star based on these values.

The far-UV spectra of our sample are shown in Fig. 1, along with our models (described in § 3). They are mainly dominated by two strong P-Cygni features - O VI $\lambda \lambda 1032, 38$ and Ne VII $\lambda 973$. Both features are saturated in the spectra of NGC 2371 and A78, while they are unsaturated in that of K 1-16. The numerous absorption lines seen are due to the Lyman

and Werner bands of molecular hydrogen (H_2), which resides in both the interstellar and circumstellar medium (discussed in HB04).

Close inspection of the Ne VII P-Cygni profile reveals that there does appear to be some absorption due to C III $\lambda 977$ in each case, as well as emission in the case of NGC 2371. This apparently arises from absorption by cooler carbon material in the circumstellar environment, perhaps similar to the “carbon curtain” Bianchi & Grewing (1987) invoked to explain the similar C II $\lambda \lambda 1334.5, 1335.7$ features seen in the spectra of NGC 40 (that CSPN has a temperature of $T_{eff} = 90 \text{ kK}$, as estimated from the UV spectrum, too hot for C II to be present in the stellar atmosphere).

3. MODELING

To analyze the spectra of our sample, we have computed non-LTE line-blanketed models which solve the radiative transfer equation in an extended, spherically-symmetric expanding atmosphere. The models are identical to those described in HB04, except neon is now included in the model atmospheres. The reader is referred to that work for a more detailed description of the models, here we give only a summary.

The intense radiation fields and low wind densities of CSPN invalidate the assumptions of local thermodynamic equilibrium, and their extended atmospheres necessitate a spherical geometry for solving the radiative transfer equation. To model these winds, we have used the CMFGEN code (Hillier & Miller 1998, 1999; Hillier et al. 2003). The detailed workings of the code are explained in the references therein. To summarize, the code solves for the non-LTE populations in the co-moving frame of reference. The fundamental photospheric/wind parameters include T_{eff} , R_* , \dot{M} , the elemental abundances and the velocity law (including v_∞). The *stellar radius* (R_*) is taken to be the inner boundary of the model atmosphere (corresponding to a Rosseland optical depth of ~ 20). The temperature at different depths is determined by the *stellar temperature* T_* , related to the luminosity and radius by $L = 4\pi R_*^2 \sigma T_*^4$, whereas the *effective temperature* (T_{eff}) is similarly defined but at a radius corresponding to a Rosseland optical depth of $2/3$. The luminosity is conserved at all depths, so $L = 4\pi R_{2/3}^2 \sigma T_{eff}^4$. We assume what is essentially a standard velocity law $v(r) = v_\infty (1 - r_0/r)^\beta$ where r_0 is roughly equal to R_* , and $\beta = 1$.

For the model ions, CMFGEN utilizes the concept of “superlevels”, whereby levels of similar energies are grouped together and treated as a single level in the rate equations (Hillier & Miller 1998). Ions and the number of levels and superlevels included in the model calculations are listed in Table 2. The atomic data references are given in HB04, except for neon (discussed in § 3.2). The parameters of the models presented here are given in Table 3.

3.1. Abundances

Throughout this work, the nomenclature X_i represents the mass fraction of element i , “ X_\odot ” denotes the solar abundance, with the values for “solar” taken from Grevesse & Sauval (1998) (their solar abundance of neon is 1.74×10^{-3} by mass). As explained in HB04, an abundance pattern of $X_{He}, X_C, X_O = 0.54, 0.36, 0.08$ was adopted to model these hydrogen deficient objects. The nitrogen abundance was taken to be $X_N = 0.01$, and solar values were adopted for the other elements, except for iron. HB04 and Werner et al.

(2003) found a sub-solar iron abundance was required to match observations of A78, and our models of that star have $X_{Fe} = 0.03 X_{\odot}$.

3.2. Neon

The prominent far-UV Ne VII feature arises from the $2p^1P^o - 2p^2^1D$ transition. As discussed by Werner et al. (2004), there is some uncertainty in the corresponding wavelength. We adopt 973.33 Å, the value found in the Chianti database (Young et al. 2003) and which was measured by Lindeberg (1972). The corresponding lower and upper level energies are 214952.0 and 317692.0 cm^{-1} , respectively.

The neon atomic data was primarily taken from the Opacity Project (Seaton 1987; Opacity Project Team 1995, 1997) and the Atomic Spectra Database at the NIST Physical Laboratory. For Ne VII, energy level data have been taken from NIST with the exception of the $2p^2^1D$ level, for which we have used the value from the Chianti database. Individual sources of atomic data (photo-ionization and cross-sections) include the following: Luo & Pradhan (1989) (Ne V), Tully et al. (1990) (Ne VII), and Peach et al. (1988) (Ne VIII).

4. RESULTS

The goal of this work was to test whether the inclusion of neon in the models of HB04 could account for the strong P-Cygni feature appearing at ~ 975 Å in the spectra of two transition stars (NGC 2371 and A78), which previously has lacked a plausible explanation (HB04). The previous common identification with C III $\lambda 977$ was questioned by HB04, as the presence of this ion would imply a much lower T_{eff} , inconsistent with other spectral diagnostics. Koesterke & Werner (1998) speculated that for A78, neglected iron lines might sufficiently cool the outer layers of the (otherwise hot) wind to allow for the formation of C III. However, HB04 computed models which included highly ionized iron, and excluded this explanation for the observed feature. As we discuss below, we find that this P-Cygni line originates from Ne VII in both stars. We also show that this is the case for a PG 1159 star, K 1-16. Additionally, we explore the usefulness of this feature as a diagnostic for stellar parameters, which is very important given the scarcity of diagnostic lines at high effective temperatures (discussed by HB04).

4.1. NGC 2371 & A78

We initially re-calculated the NGC 2371 and A78 best-fit models of HB04 (Table 3) including neon at solar abundance. The resulting models reproduced the $\lambda 973$ P-Cygni feature at a strength comparable to the observations, (although a bit weak in both cases), showing that Ne VII is indeed responsible for this line. We also computed models with higher neon abundances, which is a predicted consequence of the “born-again” scenario (see § 4.3). In Fig. 1, we show the $X_{Ne} = 10 X_{\odot}$ models, which are nearly indistinguishable from the solar abundance models (see § 4.3). We have applied the effects of H I and H₂ absorption to the model spectra as described in HB04. The feature is weaker in the observations of A78 than in those of NGC 2371, and its blue P-Cygni edge is more severely affected by absorption from H₂, making assessments of the quality of its model fit more uncertain. We note here that the parameters derived by HB04 were determined from a variety of diagnostic lines, and the listed uncertainties take into account all the different adjustments needed to fit them all, not just the ones shown here. In addition, the inclusion of neon in the calculation does not change the ionization

significantly for other abundant ions in the wind (as can be seen in Fig. 1, where the HB04 models are also plotted), thus there was no need for a revision of the stellar parameters.

4.2. K 1-16

Based on the similar parameters (T_{eff} and abundances) of NGC 2371 and A78 to those of PG 1159 stars discussed by Werner et al. (2004), we suspected that the broad P-Cygni profile identified therein as C III $\lambda 977$ in the spectra of a few of their objects originated from Ne VII as well. Werner et al. (2004) do classify a Ne VII line from their (static) models, but only attribute this identification to a narrow absorption feature, while identifying the broad P-Cygni wind feature as C III.

We decided to test this hypothesis for the case of the PG 1159 star K 1-16. Koesterke & Werner (1998) determined the following parameters for K 1-16 from a hydrostatic analysis: $T_* = 140$ kK, $\log L/L_{\odot} = 3.6$ (which imply $R_* = 0.11 R_{\odot}$), $\log g = 6.1$, X_{He} , X_C , $X_O = 0.38, 0.56, 0.06$, and the following parameters from a wind-line analysis: $v_{\infty} = 4000$ km s^{-1} and $\log \dot{M} = -8.1 M_{\odot} \text{ yr}^{-1}$ from the O VI resonance lines. Although the mass-loss rate is lower, the other parameters are close to those NGC 2371, so we first took the parameters of our NGC 2371 model shown in Fig. 1, and scaled them to K 1-16’s radius of $R_* = 0.11 R_{\odot}$ as determined by Koesterke & Werner (1998). Further scaling of the model flux is needed to match the observed flux levels of K 1-16, and this scaling is equivalent to the star lying at a distance of 2.05 kpc. The only distance estimates to this star are statistical (based on nebular relations), ranging from 1.0 to 2.5 kpc (Cahn et al. 1992; Maciel 1984, respectively). The FUSE spectrum of K 1-16 (Fig. 1) shows a unsaturated O VI P-Cygni profile of comparable strength to the Ne VII feature (which is also unsaturated), in contrast to that of NGC 2371, where the profiles are saturated and that of O VI is stronger than that of Ne VII. We therefore decreased the mass-loss rate of the scaled model with solar neon abundance until the O VI feature was fit adequately (the resulting parameters of the best-fit model for K 1-16 are listed in Table 3). The resulting model’s Ne VII feature is unsaturated and is weak compared to the observations, as shown in Fig. 2. We also computed an enriched model with $X_{Ne} = 10 X_{\odot}$ (also shown). As the figure illustrates, the feature (unsaturated in this case) is now very sensitive to the abundance (unlike the cases of NGC 2371 and A78), and the profile of the Ne-enriched model is now too strong. Fig. 1 shows both the Ne VII and O VI lines of the Ne-enriched K 1-16 model.

Our models undoubtedly show that Ne VII, not C III, accounts for the broad P-Cygni profile seen in the PG 1159 stars as well. Furthermore, our models demonstrate how this feature can be used to detect a supersolar neon abundance in the case of an unsaturated Ne VII $\lambda 973$ profile. Although these results suggest a supersolar abundance for K 1-16, a more complete photospheric/wind-line analysis should be performed, given that other parameters influence the strength of this line (§ 4.3).

To account for the interstellar H I absorption, we have used the H I parameters utilized by Kruk & Werner (1998) ($\log N(\text{H I}) = 20.48 \text{ cm}^{-2}$, $b = 20 \text{ km s}^{-1}$). We modeled the H₂ absorption using $\log N(\text{H}_2) = 16.0 \text{ cm}^{-2}$, which produces fits adequate for our purpose (Figs. 1 and 2). We have assumed H I and H₂ gas temperatures of 80 K, and used the same methods described in HB04 to calculate the absorption profiles. We found a slightly higher reddening value

than that of Kruk & Werner (1998) to produce better results ($E_{B-V} = 0.025$ vs. 0.02 mag). We note that the far-UV spectrum of K 1-16 shows very little absorption from H_2 compared to other CSPN (*e.g.*, Herald & Bianchi 2002, 2004a,b), presenting a very “clean” example of a far-UV CSPN spectrum.

4.3. Ne VII $\lambda 973$ as a DIAGNOSTIC

To investigate the potential of this feature as a diagnostic of stellar parameters, we computed exploratory models varying either the neon abundance, the mass-loss rate or the temperature of the A78 and NGC 2371 models (while keeping the other parameters the same) to study the sensitivity of this line to each parameter.

Evolutionary calculations of stars experiencing the “born-again” scenario (*e.g.*, see Herwig 2001) predict a neon abundance of $\sim 2\%$ by mass in the intershell region, produced via $^{14}\text{N}(\alpha, \gamma)^{18}\text{F}(e^+\nu)^{18}\text{O}(\alpha, \gamma)^{22}\text{Ne}$. This material later gets “dredged up” to the surface, resulting in a surface abundance enhancement of up to 20 times the solar value. We have thus calculated models with super-solar neon abundances (with $X_{\text{Ne}} = 10 X_{\odot}$, and $50 X_{\odot}$) to gauge the effects on the $\lambda 973$ feature (shown in Fig. 3). As expected, because the feature is nearly saturated in both cases, the line shows only a weak dependence on X_{Ne} . The enriched models do result in a better fit than the solar abundance models. However, given the sensitivity of this line to T_{eff} (discussed below) and the uncertainty in this parameter (see HB04), we cannot make a definitive statement about the neon abundance of these transition objects based solely on this wind line. On the other hand, the strength of the Ne VII line depends dramatically on the neon abundance in parameter regimes where it is not saturated, *e.g.*, for very high T_{eff} or very low mass-loss rates, as discussed below and shown in Figs. 2-4.

To test the sensitivity of the $\lambda 973$ feature to \dot{M} , we have computed a range of models varying the mass-loss rates of our models (with solar neon abundance) while keeping the other parameters fixed for each. We find virtually no change while the $\lambda 973$ profile remains saturated, until the change in \dot{M} induces a significant change in the ionization of the wind. This is shown for the model parameters of K 1-16 in Fig. 4, where the Ne VII profile is essentially unchanged for $5 \times 10^{-8} < \dot{M} < 1 \times 10^{-7} M_{\odot} \text{ yr}^{-1}$, and then weakens dramatically as \dot{M} lowered to $1 \times 10^{-8} M_{\odot} \text{ yr}^{-1}$. However, if the atmosphere is Ne-enriched, this limit could be significantly lower, as illustrated in the $5 \times 10^{-9} M_{\odot} \text{ yr}^{-1}$ ($T_{\text{eff}} = 135$ kK) case.

The ionization structures of neon for the A78 and NGC 2371 models (with $X_{\text{Ne}} = 1 X_{\odot}$) are shown in Fig. 5. In the cooler A78 model, Ne VII is only dominant deep in the wind, with Ne VI being dominant in the outer layers. We have explored the temperature sensitivity of the feature by adjusting the luminosity of our default models while keeping the other parameters (*i.e.*, R_* and \dot{M}) the same. The results are shown in Fig. 3. For the A78 model parameters, the Ne VII $\lambda 973$ wind feature weakens as the temperature is decreased, becoming insignificant for $T_{\text{eff}} \lesssim 85$ kK. For the NGC 2371 model parameters, it weakens significantly as the temperature is lowered from $\simeq 130$ kK to $\simeq 110$ kK. The profile is fairly constant for $130 \lesssim T_{\text{eff}} \lesssim 145$ kK, and then starts to weaken as the temperature is increased, as Ne VII ceases to be dominant in the outer wind (around $T_{\text{eff}} \simeq 150$ kK), and becomes a pure absorption line for $T_{\text{eff}} \gtrsim 170$ kK. However, these thresholds are dependent on the neon abundance, as illustrated by the $T_{\text{eff}} = 165$ kK models. For that temperature,

the solar neon abundance model shows only a weak, unsaturated P-Cygni profile, but in the $X_{\text{Ne}} = 10 X_{\odot}$ model, the line increases dramatically, becoming saturated again. This shows the potential of this line to exist in strength over a wide range of effective temperatures, as well as being an Ne-abundance diagnostic. The presence of Ne VII as a P-Cygni profile sets a lower limit to T_{eff} (~ 80 kK), quite independent of the neon abundance.

Although our modeling indicates the Ne VII $\lambda 973$ feature may not be useful in diagnosing a super-solar neon abundance in the case of NGC 2371 (because it is saturated) and A78 (because its blue edge is obscured by H_2 absorption), it does show other neon transitions in the far-UV and UV which do not produce significant spectral features for a solar neon abundance, but do for enriched neon abundances (see examples in Fig. 6). The strongest examples are the $\lambda 2213.13$ and $\lambda 2229.05$ transitions from the $3d^2D - 3p^2P^o$ Ne VI triplet which become evident in models of both objects when $X_{\text{Ne}} = 10 X_{\odot}$. For this abundance, Ne VI $3p^2P^o - 3s^2S$ transitions are also seen at $\lambda 2042.38$ and $\lambda 2055.94$ in the A78 models, and the Ne VII $3s^1S - 3p^1P^o$ transition ($\lambda 3643.6$) in the models of NGC 2371 (this line has been used by Werner & Rauch 1994 to deduce enhanced neon abundances in a few PG 1159 stars, including K 1-16). Also seen in the $X_{\text{Ne}} = 10 X_{\odot}$ models of NGC 2371 is the Ne VII $3p^3P^o - 3d^3D$ multiplet, which Werner et al. (2004) observed at positions shifted about 6 \AA blueward of the wavelengths listed in the NIST database (the strongest observed component occurs at $\lambda 3894$). For $X_{\text{Ne}} = 50 X_{\odot}$, in the model of NGC 2371, Ne VI $2p^2^4P - 2p^2^2P^o$ features are seen from 993 \AA to 1011 \AA , as well as blend of Ne V- Ne VII transitions at $\sim 2300 \text{ \AA}$. Although the resolution and/or quality of the available IUE data in this range are not sufficient to rigorously analyze these lines, we note that the observations seem to favor a higher neon abundance, based on a significantly strong feature at 2230 \AA in the IUE observations of NGC 2371 that is only matched by the $X_{\text{Ne}} = 50 X_{\odot}$ model.

We note that introducing neon at solar abundance in the model atmospheres of these objects does not have a significant impact on the ionization structure of other relevant ions in the wind. For A78, at $X_{\text{Ne}} = 10 X_{\odot}$, the ionization structures of other elements changes slightly, but not enough to result in spectral differences. Very high neon abundances ($X_{\text{Ne}} = 50 X_{\odot}$) result in a less ionized wind, with, for example, the O V $\lambda 1371$ feature strengthening as this ion becomes more dominant in the outer parts of the wind. The neon ionization structure is most dramatically affected - with Ne V becoming the dominant ion in the outer parts of the wind. For NGC 2371, introducing neon at solar abundance reduces the ionization of the wind slightly, with the effect becoming more significant at $X_{\text{Ne}} \geq 10 X_{\odot}$ when it leads to stronger N V and O V features at UV wavelengths. Thus, high neon abundances can significantly influence the atmospheric structure, and fitting a spectrum using the same set of non-neon diagnostics with a model with an enriched neon abundance generally seems to require a higher luminosity.

5. CONCLUSIONS

We have shown that the strong P-Cygni wind feature seen around 975 \AA (hitherto unidentified or mistakenly identified as C III $\lambda 977$) in the far-UV spectra of very hot ($T_{\text{eff}} \gtrsim 100$ kK) CSPN can be reproduced by models which include neon in the stellar atmosphere calculations. We have demon-

strated this identification in the case of A78, a transitional [WO]-PG 1159 star, and in a similar object with winds of even higher ionization, NGC 2371. Through a comparison of our models with the far-UV spectrum of the PG 1159-type CSPN K 1-16, we have also demonstrated that the broad wind feature seen at this wavelength in some PG 1159 objects originates not from C III (as indicated in Werner et al. 2004), but from Ne VII as well.

Our grid of models show that Ne VII $\lambda 973.33$ is a very strong wind feature detectable at solar abundance levels, in contrast to photospheric optical neon features (Werner et al. 2004), in CSPN of high stellar temperatures ($T_{\text{eff}} \gtrsim 85$ kK). For the parameters of NGC 2371 ($\log \dot{M} = -7.1$ $M_{\odot} \text{ yr}^{-1}$) and A78 ($\log \dot{M} = -7.3$ $M_{\odot} \text{ yr}^{-1}$), the strength of the feature peaks for $130 \lesssim T_{\text{eff}} \lesssim 145$ kK, and weakens dramatically for $T_{\text{eff}} \gtrsim 160$ (these cutoffs depend on the value of \dot{M} and the neon abundance). For an enhanced neon abundance ($X_{\text{Ne}} = 10 X_{\odot}$), the feature remains strong even in models of very high temperatures ($T_{\text{eff}} \gtrsim 165$ kK) or very low mass-loss rates ($\dot{M} \simeq 1 \times 10^{-8}$ $M_{\odot} \text{ yr}^{-1}$), while the lower T_{eff} limits remains approximately the same. We note here that the far-UV spectra of these objects show the Ne VII feature being weaker than the O VI line, while in some PG 1159 stars (e.g., K 1-16 and Longmore 4), they are of comparable strength. Since PG 1159 stars represent a more advanced evolutionary stage when the star is getting hotter and the wind is fading, Ne VII $\lambda 973$ may be the last wind feature to disappear if the atmosphere is enriched in neon.

In hydrogen-deficient objects, an enhanced neon abundance lends credence to evolutionary models which have the star experiencing a late helium shell flash, and predict a neon enrichment of about 20 times the solar value. When saturated (e.g., in the case in NGC 2371), the feature is insensitive to \dot{M} , and only weakly sensitive to the neon abundance. Although models of these objects with enriched neon abundances do result in better fits for our transition objects, the sensitivity of the feature to T_{eff} prevents us making a quantitative statement regarding abundances based on this feature alone. Other far-UV/UV lines from Ne VI (at 2042, 2056, 2213, and 2229 Å) and Ne VII (at 3644 Å) which only appear in Ne-enriched models, could in principle be used for this

purpose, but we lack observations in this range of sufficient quality/resolution to make a quantitative assessment. In the case of K 1-16, Ne VII $\lambda 973$ is unsaturated, and our models require an enhanced neon abundance to fit it simultaneously with the O VI $\lambda \lambda 1032, 38$ profile. This result is in line with those of Werner & Rauch (1994), who derived a neon abundance of 20 times the solar value for this object from analysis of the Ne VII $\lambda 3644$ line. The neon overabundance is further evidence that this PG 1159 object has experienced the “born-again” scenario.

Ne VII $\lambda 973$ has diagnostic applications not only to late post-AGB objects, but also for evolved massive stars. Evolutionary models predict the surface neon abundance to vary dramatically as Wolf-Rayet stars evolve (see, e.g., Meynet & Maeder 2005). For cooler WR stars (such as those of the WN-type), the neon abundance can be estimated from low-ionization features in the infrared and ultraviolet (e.g., [Ne II] 12.8 μm , [Ne III] 15.5 μm , Ne III $\lambda 2553$). The Ne VII $\lambda 973$ feature may provide a strong neon diagnostic for hotter, more evolved WR stars. For example, the WO star Sanduleak 2 has $T_* \simeq 150$ kK (Crowther 2000), and appears to have a feature at that wavelength in a FUSE archive spectrum. Neon enhancements produced in massive stars may explain the discrepancy in the $^{22}\text{Ne}/^{20}\text{Ne}$ ratio between the solar system and Galactic cosmic ray sources (see, e.g., Meynet et al. 2001).

We are grateful to the anonymous referee for a careful reading of the manuscript and their constructive comments. We are indebted to the members of the Opacity Project and Iron Project and to Bob Kurucz for their continuing efforts to compute accurate atomic data, without which this project would not have been feasible. The SIMBAD database was used for literature searches. This work has been funded by NASA grants NAG 5-9219 (NRA-99-01-LTSA-029) and NAG-13679. The BEFS and IUE data were obtained from the Multimission Archive (MAST) at the Space Telescope Science Institute (STScI). STScI is operated by the Association of Universities for Research in Astronomy, Inc., under NASA contract NAS5-26555.

REFERENCES

- Acker, A., Marcout, J., Ochsenbein, F., Stenholm, B., & Tylenda, R. 1992, Strasbourg-ESO Catalogue of Galactic Planetary nebulae (ESO Publication)
- Bianchi, L. & Grewing, M. 1987, A&A, 181, 85
- Cahn, J. H., Kaler, J. B., & Stanghellini, L. 1992, A&AS, 94, 399
- Crowther, P. A. 2000, A&A, 356, 191
- Crowther, P. A., De Marco, O., & Barlow, M. J. 1998, MNRAS, 296, 367
- Crowther, P. A., Dessart, L., Hillier, D. J., Abbott, J. B., & Fullerton, A. W. 2002, A&A, 392, 653
- De Marco, O. & Soker, N. 2002, PASP, 114, 602
- Grevesse, N. & Sauval, A. J. 1998, Space Sci. Rev., 85, 161
- Grewing, M. & Neri, R. 1990, A&A, 236, 223
- Herald, J. E. & Bianchi, L. 2002, ApJ, 580, 434
- . 2004a, ApJ, 611, 294
- . 2004b, ApJ, 609, 378
- Herwig, F. 2001, Ap&SS, 275, 15
- Herwig, F., Blöcker, T., Langer, N., & Driebe, T. 1999, A&A, 349, 5
- Hillier, D. J., Lanz, T., Heap, S. R., Hubeny, I., Smith, L. J., Evans, C. J., Lennon, D. J., & Bouret, J. C. 2003, ApJ, 588, 1039
- Hillier, D. J. & Miller, D. L. 1998, ApJ, 496, 407
- . 1999, ApJ, 519, 354
- Iben, I. & McDonald, J. 1995, in LNP, Vol. 443, White Dwarfs, ed. D. Koester & K. Werner (Heidelberg: Springer), 48
- Kaler, J. B., Stanghellini, L., & Shaw, R. A. 1993, A&A, 279, 529
- Koesterke, L. & Werner, K. 1998, ApJ, 500, 55
- Kruk, J. W. & Werner, K. 1998, ApJ, 502, 858
- Lindeberg, S. 1972, Uppsala Univ. Inst. Phys. Report UIIP-759, 1
- Luo, D. & Pradhan, A. K. 1989, Phys. Rev. B, 22, 3377
- Maciel, W. J. 1984, A&AS, 55, 253
- Meynet, G., Arnould, M., Paulus, G., & Maeder, A. 2001, Space Science Reviews, 99, 73
- Meynet, G. & Maeder, A. 2005, A&A, 429, 581
- Morgan, D. H., Parker, Q. A., & Cohen, M. 2003, MNRAS, 346, 719
- Opacity Project Team. 1995, The Opacity Project, Vol. 1 (Bristol: Institute of Physics Publications)
- . 1997, The Opacity Project, Vol. 2 (Bristol: Institute of Physics Publications)
- Peach, G., Saraph, H. E., & Seaton, M. J. 1988, Phys. Rev. B, 21, 3669
- Peña, M., Hamann, W.-R., Ruiz, M. T., Peimbert, A., & Peimbert, M. 2004, A&A, 419, 583
- Seaton, M. J. 1987, Phys. Rev. B, 20, 6363
- Tully, J. A., Seaton, M. J., & Berrington, K. A. 1990, Phys. Rev. B, 23, 3811
- Werner, K., Dreizler, S., Koesterke, L., & Kruk, J. W. 2003, in IAU Symp., Vol. 209, Planetary Nebulae: Their Evolution and Role in the Universe, ed. M. Dopita & S. Kwok (San Francisco: ASP), 239
- Werner, K. & Rauch, T. 1994, A&A, 284, 5
- Werner, K., Rauch, T., Reiff, E., Kruk, J. W., & Napiwotzki, R. 2004, A&A, 427, 685

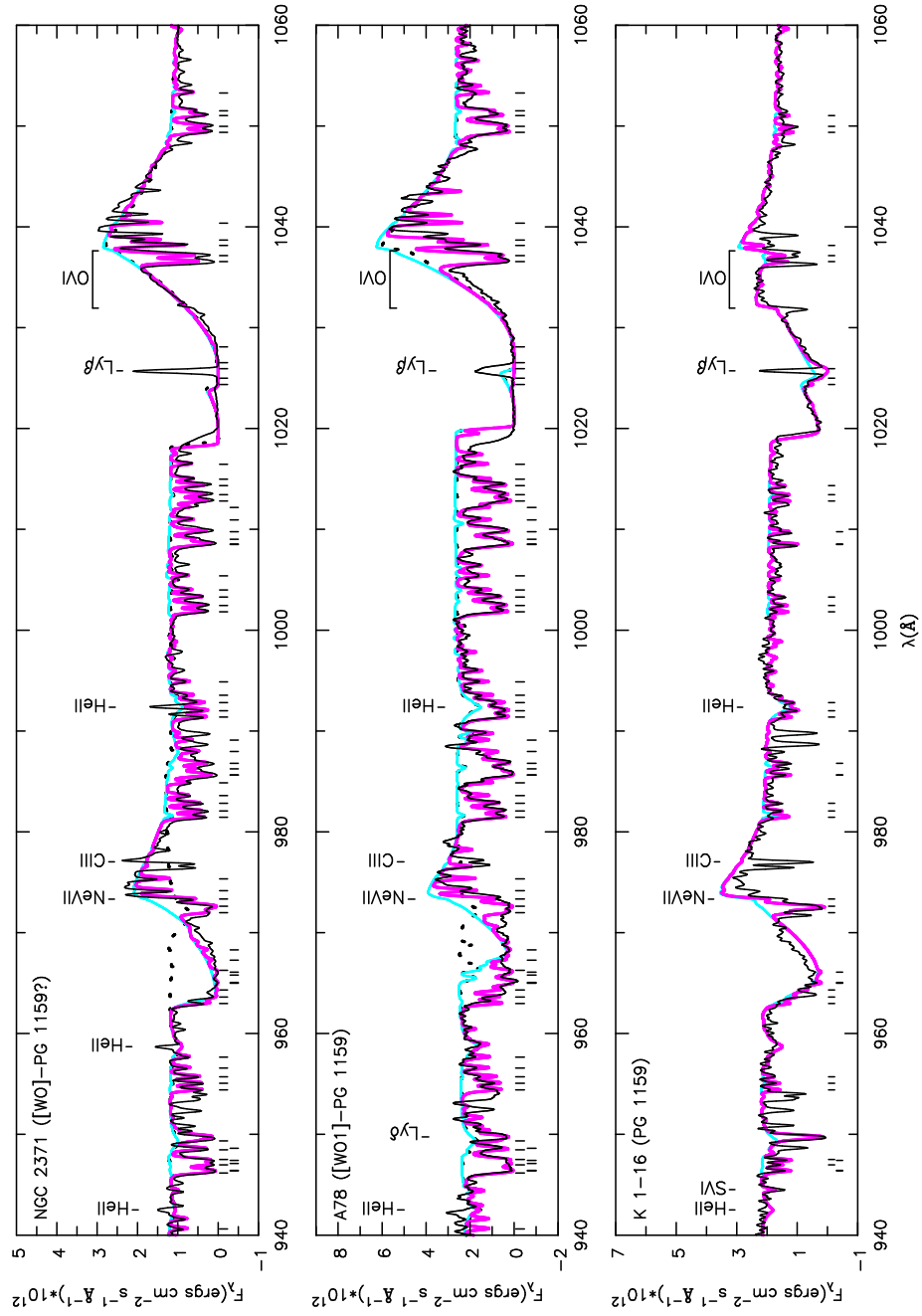


FIG. 1.— The FUSE observations (black) along with our stellar models (with $X_{Ne} = 10 X_{\odot}$), both with (pink/dark gray) and without (aqua/light gray) the effects of the hydrogen absorption models applied (see text). The models indicate Ne VII to be responsible for the P-Cygni feature seen at ~ 975 Å. We also show the original HB04 models of NGC 2371 and A78 (black dotted), which did not include neon in the model atmospheres.

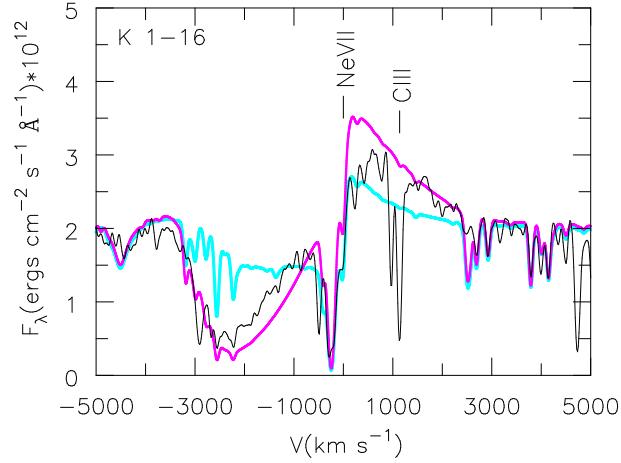


FIG. 2.— FUSE spectrum of the Ne VII $\lambda 973$ profile (in velocity space) of K 1-16 (black) along with two model spectra, one with $X_{Ne} = 1 X_{\odot}$ (solar), and one with $X_{Ne} = 10 X_{\odot}$ (aqua/light gray and pink/dark gray, respectively). Effects of interstellar H I and H₂ absorption have been applied to the model spectra (§ 4.2). The unsaturated profile is very sensitive to the neon abundance, and indicates a super-solar abundance in this object.

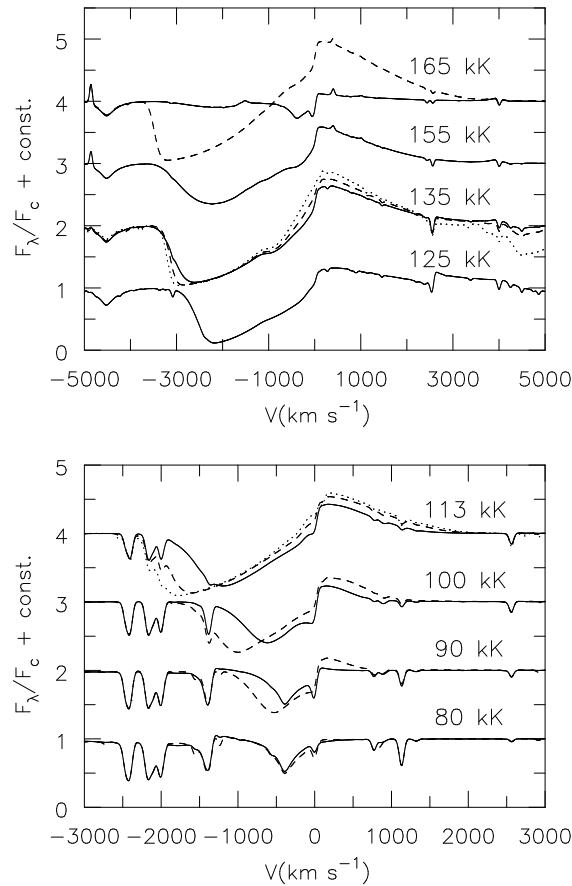


FIG. 3.— The effects of varying T_{eff} and X_{Ne} of our NGC 2371 model (top) and A78 model (bottom) on Ne VII $\lambda 973$. The solid, dashed, and dotted lines represent models with neon abundances of $1 X_{\odot}$ (solar), $10 X_{\odot}$, and $50 X_{\odot}$, respectively. When saturated (e.g., in the $T_{eff} = 135$ kK model), the feature is not very sensitive to X_{Ne} . It is sensitive to T_{eff} , and becomes pure absorption for $T_{eff} \lesssim 85$ kK and is of significant strength for $100 \lesssim T_{eff} \lesssim 160$ kK. The feature is weak in the solar neon abundance $T_{eff} = 165$ model, but strengthens dramatically when $X_{Ne} = 10 X_{\odot}$, illustrating the abundance sensitivity of the line in some parameter regimes where it is unsaturated. The spectra are normalized (and in velocity space), and convolved with a 0.2 \AA Gaussian for clarity.

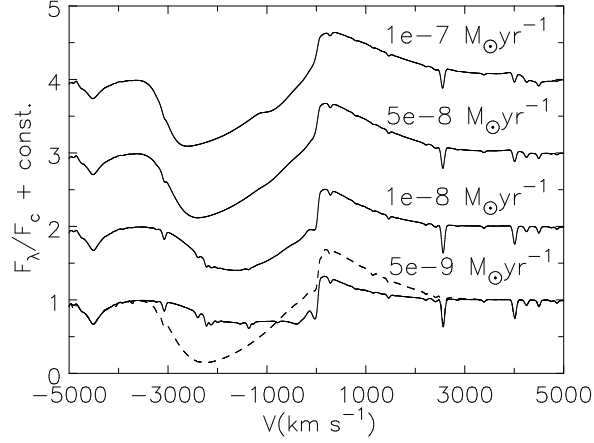


FIG. 4.— The effects of varying \dot{M} and X_{Ne} of our K 1-16 model ($T_{\text{eff}} = 135$ kK, $R_* = 0.11 R_{\odot}$) on Ne VII $\lambda 973$. The solid and dashed lines represent models with neon abundances of $1 X_{\odot}$ (solar) and $10 X_{\odot}$, respectively. The feature is very sensitive to \dot{M} when not saturated (e.g., the $\dot{M} = 5 \times 10^{-9} M_{\odot} \text{yr}^{-1}$ model). The spectra are normalized, and convolved with a 0.2 \AA Gaussian for clarity.

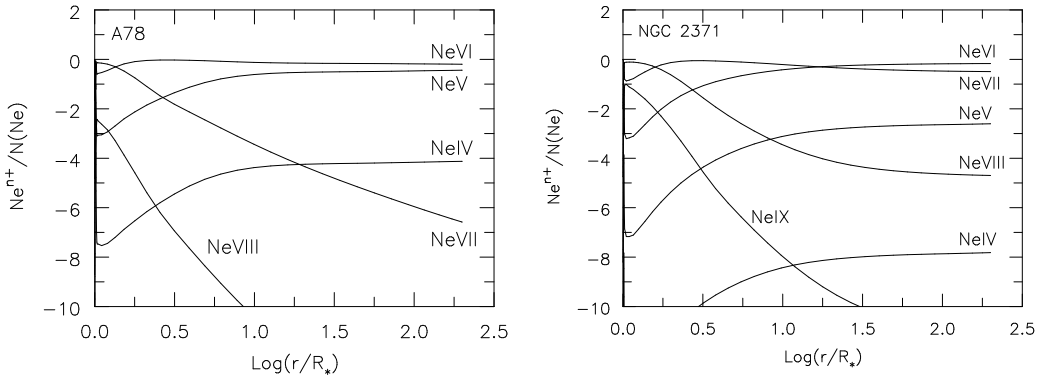


FIG. 5.— The neon ionization structures of our models for A78 ($T_{\text{eff}} \simeq 115$ kK) and NGC 2371 ($T_{\text{eff}} \simeq 135$ kK) as a function of distance from the stellar surface. For the cooler object, Ne VII is only dominant deep in the wind, while in the hotter model it is dominant further out.

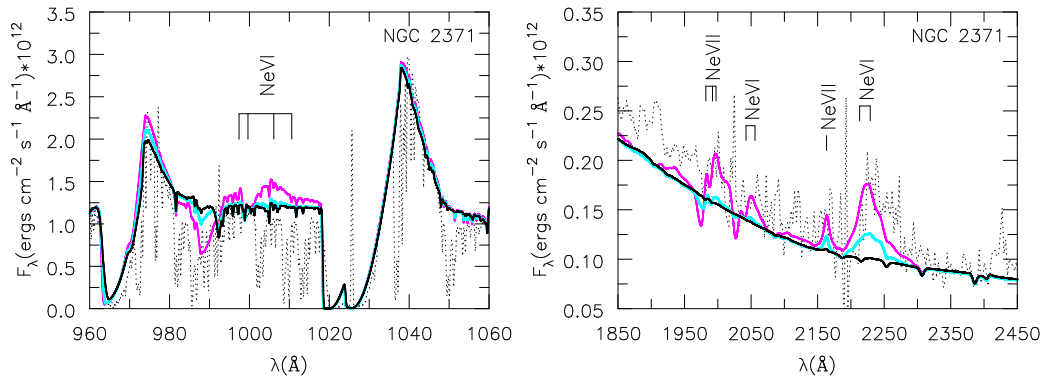


FIG. 6.— Additional neon diagnostics: The NGC 2371 FUSE (left) and IUE (right) observations are shown (dotted) along with models with $X_{\text{Ne}} = 1 X_{\odot}$ (black), $X_{\text{Ne}} = 10 X_{\odot}$ (aqua/light gray) and $X_{\text{Ne}} = 50 X_{\odot}$ (pink/dark gray). The labeled features are not apparent in the solar abundance model, but become significant as the neon abundance is increased.

TABLE 1
UTILIZED SPECTRA

| Star | Instrument | Data-set | Date | Resolution | Aperture ($''$) | Range (\AA) |
|----------|------------|-------------|----------|-------------------------|----------------------|---------------------------|
| NGC 2371 | FUSE | P1330301 | 02/26/00 | $\sim 0.05 \text{ \AA}$ | 30×30 | 915–1180 |
| | IUE | LWR04210 | 04/07/79 | 5–6 \AA | 10×20 | 1975–3345 |
| Abell 78 | BEFS | BEFS2190 | 12/01/96 | $\sim 0.33 \text{ \AA}$ | 20 | 915–1222 |
| K 1-16 | FUSE | M1141201002 | 07/24/00 | $\sim 0.05 \text{ \AA}$ | 30×30 | 915–1180 |

TABLE 2
SUPERLEVELS AND LEVELS FOR MODEL IONS

| Element | I | II | III | IV | V | VI | VII | VIII | IX | X | XI |
|---------|-------|-------|-------|--------|--------|--------|--------|--------|--------|--------|-----|
| H | 20/30 | 1/1 | | | | | | | | | |
| He | 40/45 | 22/30 | 1/1 | | | | | | | | |
| C | | | 30/54 | 13/18 | 1/1 | | | | | | |
| N | | | | 29/53 | 13/21 | 1/1 | | | | | |
| O | | | | 29/48 | 41/78 | 13/19 | 1/1 | | | | |
| Ne | | | | 45/355 | 37/166 | 36/202 | 38/182 | 24/47 | 1/1 | | |
| Si | | | | 22/33 | 1/1 | | | | | | |
| P | | | | 36/178 | 16/62 | 1/1 | | | | | |
| S | | | | 51/142 | 31/98 | 28/58 | 1/1 | | | | |
| Fe | | | | 51/294 | 47/191 | 44/433 | 41/254 | 53/324 | 52/490 | 43/210 | 1/1 |

TABLE 3
STELLAR PARAMETERS AND ADOPTED DISTANCES

| Star | T_{eff} (kK) | v_{∞} (km s^{-1}) | D (kpc) | R_* (R_{\odot}) | $\log L$ (L_{\odot}) | $\log \dot{M}$ ($M_{\odot} \text{ yr}^{-1}$) |
|-----------------------|-------------------------------------|--|--------------|--------------------------|--|---|
| NGC 2371 ^a | 135^{+10}_{-15} | 3700 ± 200 | 1.5^b | 0.09 | $3.45^{+0.12}_{-0.20}$ | -7.11 ± 0.30 |
| Abell 78 ^a | 113 ± 8 | 3200 ± 50 | 1.6^b | 0.19 | $3.73^{+0.10}_{-0.13}$ | $-7.33^{+0.36}_{-0.13}$ |
| K 1-16 | 135 | 3700 | 2.05 | 0.11 | 3.6 | -8.3 |

(a): Stellar parameters from HB04

(b): Distance from Cahn et al. (1992)

Parameters in **bold** are those adopted for the models in this paper.